TRANSACTIONS OF THE INSTITUTE OF MEASUREMENT & CONTROL

Article

Transactions of the Institute of Measurement and Control
2019, Vol. 41(11) 3190–3198

DOI: 10.1177/0142331218824392
journals.sagepub.com/home/tim
SAGE

Design, modeling, and control of a horizontal magnetic micromanipulator

Günyaz Ablay, Mustafa Böyük and Kutay İçöz

Abstract

Magnetic micromanipulators with a wide range of force generating capabilities are able to manipulate micron size particles for various applications and measurements. These magnetic particles can be coated with receptors to specifically bind to target biomolecules. In this work, a horizontal magnetic micromanipulator is designed, modeled and controlled for single micron size magnetic particle manipulations. A method is presented for dynamic modeling of magnetic micromanipulators. A feedback control method is designed that allows direct linearization of the system. It is shown that the proposed controller guarantees the stability of the closed-loop system, and yields zero steady-state error in a wide range of operation conditions. We show that the micromanipulator is able to generate a wide range of piconewton (pN) scale forces on a superparamagnetic particle for single molecule separation, and biosensor developments.

Keywords

Modeling, control, micromanipulation, magnetic manipulator, magnetic force

Introduction

Generating molecular scale force has a crucial role for biological processes and motions such as cell separation and DNA segregation (Capitanio and Pavone, 2013). The most significant techniques developed in recent years are the magnetic micromanipulators, optical tweezers and atomic force microscopy (Neuman and Nagy, 2008). Other techniques for manipulating single molecules include micro-needle manipulation (Aziz et al., 2012), dielectrophoresis-based tweezers (Kodama et al., 2013; Luo et al., 2018), flow induced stretching (Smith et al., 1992) and biomembrane force probe (Ju and Zhu, 2017). The molecule/cell manipulation methods are in their infant stage and have a big potential for various practical applications in different fields. The general properties of the magnetic micromanipulation techniques are different than the macro-scale magnetic manipulators, for example, magnetic levitation systems (Eroğlu and Ablay, 2016). To manipulate single molecules/cells to distances ranging from nanometer to millimeter lengths, a relatively small amount of force in the range of 10^{-14}–10^{-8} N must be generated by current methods (Neuman and Nagy, 2008). Manipulation of single molecules has been performed for investigating receptor binding strength or location (Litvinov et al., 2002) and for measuring adhesion forces (Prass et al., 2006). While the early applications were used for characterization of motor proteins (Svoboda and Block, 1994), the recent applications include elasticity measurements and manipulations in nucleic acids (Fuller et al., 2006), characterization of antibody binding (Li et al., 2013), and investigation of protein multi-state unfolding (Pelz et al., 2016).

Magnetic micromanipulators offer safe operations in biological environments and precise measurements can be obtained from permanent magnets or electromagnets to produce controlled forces and torques for various applications (Gosse and Croquette, 2002; Kriegel et al., 2017; Vlaminck and Dekker, 2012). While permanent magnets offer empirical study-based simple designs and do not need any feedback control action unless motorized, electromagnets offer a variety of different design options with controlled magnetic force generations.

In general, the magnetic micromanipulators can be designed in vertical or horizontal schemes. In vertical magnetic micromanipulators, the magnetic force strength is adjusted via magnet movements (either away or closer to the sample). Some applications in the literature report the measurement of DNA molecule from the tethered bead (Huhle et al., 2015; Klaue and Seidel, 2009; Smith et al., 1992; Strick et al., 2000). The vertical magnetic micromanipulators require complex and sophisticated calibration techniques. To eliminate the calibration requirements, horizontal magnetic micromanipulators have been reported (Fabian et al., 2018; McAndrew et al., 2016; Schwarz et al., 2013; Yan et al., 2004). However, the reported designs are based on permanent-magnets and the motion of these magnets are manually controlled by electric motors.

Electrical and Electronic Engineering Department, Abdullah Gül University, Turkey

Corresponding author:
Günyaz Ablay, Electrical and Electronic Engineering Department, Abdullah Gül University, Kayseri 38080, Turkey.
Email: gunyaz.ablay@agu.edu.tr

In this work, a full automatic horizontal magnetic micromanipulator based on feedback controlled electromagnets is presented. A dynamic force model is provided based on the magnetic monopole and magnetic circuit approaches, and an automatic control method is also proposed for the horizontal magnetic micromanipulator. The powerful (robust and accurate) numerical solvers are used to quantitatively predict the magnetic forces, and systematically investigate the effects of different electromagnet geometries and configurations. Finally, a simple feedback linearizing controller is designed, and its implementation results are provided to show the effectiveness of the proposed design and control.

In the following sections, the fundamentals of magnetic particles and their applications, system modeling and control design approaches, and experimental results are provided.

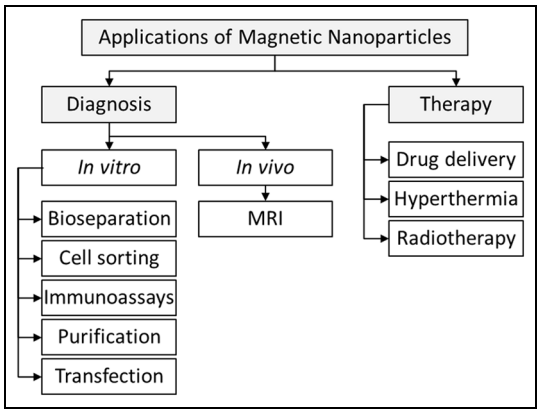

Figure 1. Usages of superparamagnetic particles.

Magnetic particles and their applications

Superparamagnetic particles are commercially produced in different sizes (from 120 nm to 10 μm), and are composed of iron oxide nanoparticles that are typically made of magnetite (Fe_3O_4) or maghemite (γ-Fe_2O_3), and polymer matrix coatings (Fonnum et al., 2005). The superparamagnetic materials are easily magnetized by external magnetic fields, but they exhibit a non-magnetic behavior in the absence of external magnetic field, namely, residual magnetization or hysteresis phenomenon does not occur. In addition, their relative magnetic permeabilities are as strong as the ferromagnetic materials.

Magnetic particles as a powerful non-invasive tool, find applications in various fields including biomedical, environmental and information storage systems (Gijs, 2004; Hermanson, 2013). Antibody-coated, streptavidin-dextran-coated and fluorescence-coated Fe_3O_4 magnetic particles are commercially available for versatile biomedical applications. As shown in Figure 1, the application areas can be grouped into two fields: diagnosis and therapy (Rahman et al., 2015). Below, some of the significant biomedical applications of superparamagnetic particles will be summarized.

Magnetic separation

Magnetic particles such as superparamagnetic particles have been used for separation of cells or molecules because of their small size, good dispersibility, and promising separation mood. One common magnetic separation method is based on antibodies conjugated particles that can specifically bind to their matching antigens on the surface of the target. To separate the labeled entities, a suitable external magnetic field must be applied to attract and carry the magnetically labeled entities in specific regions. In this way, separation of tumor cells from blood, isolation of certain enzymes, and extraction of DNA/RNA from body fluids can be possible (Plouffe et al., 2015).

Diagnostics

The superparamagnetic nanoparticles can be used to enhance magnetic resonance imaging (MRI) contrast. The applied magnetic field causes a small fraction of protons to line up parallel to the field. Once the magnetic field is turned off, the amplitudes of magnetic moments relax back to their initial values. During this relaxation, the signal variation is measured. The magnetic nanoparticles are used to reduce this relaxation time of protons. If the relaxation time in a region tagged by magnetic particles is lower than the untagged regions, a strong contrast is obtained. This is the basis of the MRI contrast enhancement between the different types of cells (Kim et al., 2003; Lawaczeck et al., 1997). This method can be used to diagnose malignant tumors (Agostini et al., 2016).

Therapy

Magnetic nanoparticles can be used to kill malignant cells by heating the target tissue to temperatures around 43°C. This targeted treatment technique is known as hyperthermia. The principle of the concept is based on the heating of magnetic particle by hysteresis loss when located in a high frequency (~1 MHz) magnetic field (Stauffer et al., 1984). The heating mechanism for ferromagnetic materials can be explained with hysteresis losses, while for superparamagnetic particles the heating can occur by the rotation of the particles (Rosensweig, 2002). It is possible to apply the magnetic particle heating any depth in the human body for the treatment of tumors. In addition, magnetic nanoparticle hyperthermia can also be used as an adjuvant therapy method for chemotherapy and radiotherapy.

Drug delivery

Chemotherapy is a non-specific method because the drugs are not specifically distributed to the required areas (resulting in undesirable side-effects). On the other hand, magnetic nanoparticles have been developed for localizing drug delivery to tumors (Tietze et al., 2015). The magnetic nanoparticle behaves like a drug carrier. The drug is attached to the outer surface of the magnetic particle, or it is dissolved in the coating. First, the drug coated magnetic particles are introduced into the bloodstream of patient, and then the external

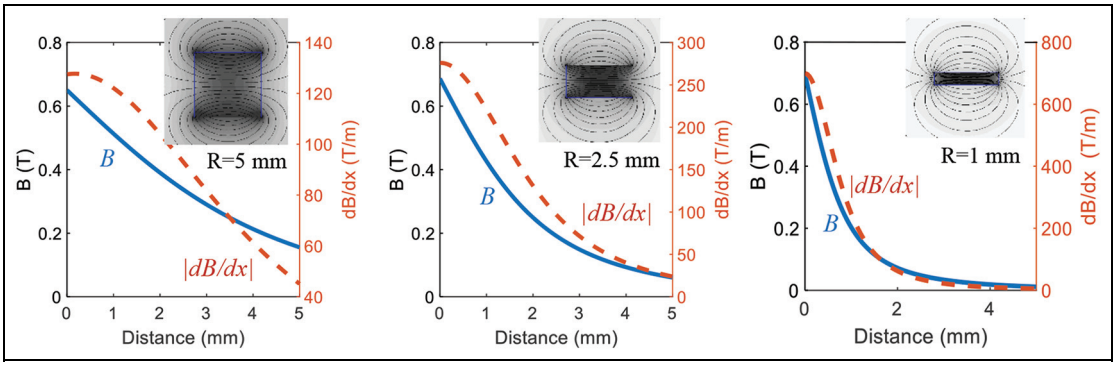

Figure 2. Magnetic field and field gradient variations with magnet size.

magnetic field is applied to retain these particles at the specified region. Finally, the drug is released via an enzymatic activity or a controlled triggering mechanism. In addition, radionuclides such as β–emitters can be bonded to the magnetic particles for targeted delivery.

Sensors

Magnetic particles have different composition, size, and magnetic properties. Using these features of magnetic particles, the biosensors can be functionalized to recognize specific molecular targets, and a time and cost-efficient signal amplification can be achieved. Magnetic particles are linked to other molecular labels such as antibody to improve sensitivity and provide signal amplification for the biological measurements (İçöz and Mzava, 2016; Icoz and Savran, 2010). The sensitivity and signal amplification of biosensors can be used to address some unmet clinical needs, such as discriminating benign prostatic hypertrophy from prostate cancer via a piezoelectric/magnetic particle-based assay (Jokerst et al., 2015).

Artificial muscle

Artificial muscles can be developed from soft actuators including ferrogels, magnetic gels, magnetic field sensitive gels, magnetorheological elastomers, and magnetoactive polymers (Nguyen et al., 2012). These materials contain magnetic nanoparticles such that the particles respond to the external magnetic field and change the position of the surrounding polymer chain, hence the overall shape of the composite changes. By designing and using a suitable magnetic actuator, different actuation mode for the artificial muscle can be obtained such as elongation, contraction, deflection, and coiling.

System modeling and controller design

System and device

A magnetic micromanipulator generates an external force on the superparamagnetic particle proportional to the gradient of the square of the magnetic field. Large magnets generate strong magnetic fields, but weak field gradient, and thus

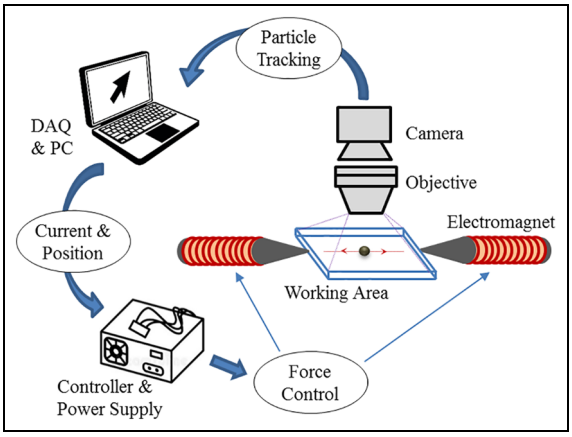

Figure 3. Horizontal magnetic micromanipulator setup.

slowly changing forces in a large area. It is possible to produce strong magnetic forces and sharp field gradients with small magnets, but the magnetic force diminishes fast with the distance. Figure 2 illustrates these features for different sizes of N52 grade neodymium magnets (where R is the radius), and these results are compatible with electromagnets. Hence, it is desirable to apply magnetic force in the close neighborhood of magnets. Magnetic force can be produced by single or multiple electromagnets. To meet different application requirements of single-molecule manipulation, such as spatial control and torque production, different configurations of electromagnets should be considered.

In this work, a horizontal micromanipulator system is designed, as illustrated in Figure 3. In the design, we have considered the significant factors related to the magnetic particle behavior. There are key factors affecting the behavior of magnetic particles in a fluidic environment. Some of these factors can be observed and controlled. Viscosity, size, and magnetic content of the particle, temperature and ionic force effect, and magnetic force have direct impact on the designs. To produce adequate magnetic force to attract the particle, the electromagnets are strengthened with ferromagnetic core structures in the designs. The core is constructed with soft iron or steel for generating strong magnetic forces. In addition, in the design the effects of material saturation and hysteresis (and

possible heating issue) are taken into account for healthy operations. A camera attached microscope system is used to detect and measure the position of the magnetic particles.

Fluidic reservoir (working area) is made of Polymethyl methacrylate (PMMA) material, a plastic material known as Plexiglas. A piece of PMMA is cut and shaped using a laser cutter, and then placed in the central area of the magnetic pole tips. A motorized manipulator used to adjust position of micromanipulator and camera system in xyz directions. The fine motor resolution, around several micrometers, allows focusing on particles with different sizes. For data acquisition and processing, a workstation equipped with high performance CPU and Matlab software is used. An image-based particle detection and tracking system is developed in Matlab. Center of mass particle detection and tracking algorithm is developed, and a threshold filter is used to separate the brightness differences between the particle and the background. For actuating and controlling the electromagnets, microcontrollers, power mosfet drivers and adjustable DC power supplies are used.

In general, a feedback control mechanism is needed to be developed for precise and fast control actions. The effective stiffness of the magnetic micromanipulator is determined by feedback control system. For analysis, calibration and control design goals, the first principles approach is used to obtain the system model. This model is also used to calculate the force and current needs, and to estimate the control parameters.

Magnetic particle dynamics

By considering Newton's second law of motion and independent motion in x direction, the magnetic particle dynamics in fluidic environment is given by

$$m\ddot{x} + \sigma\dot{x} = F_x + F_t + F_g + F_o \tag{1}$$

where m(in kg) is the mass of the particle, σ(in Ns/m) is the drag coefficient of the particle in aqueous solution, F_x, F_t, F_g and F_o(in N) are the magnetic force, thermal force, gravity force, and other forces, respectively.

According to Stokes' law (Happel and Brenner, 1983), the damping coefficient for a spherical object in a viscous fluid is given by

$$\sigma = 6\pi\eta\beta R \tag{2}$$

where η is the dynamic viscosity of the fluid (e.g. $\eta = 8.9 \times 10^{-4}$ Ns/m^2 at 25 °C for water), β is the correction factor varying as $1 \leqslant \beta \leqslant 3$, and R is the radius of the spherical particle.

F_t(in N) is the random thermal force (also known as Brownian force) due to the impacts of the molecules of the liquid on the particle. The thermal force is described with a white noise whose power spectrum density is $PSD(F_t) = 4k_BT\sigma$, where $k_B = 1.38 \times 10^{-23}$(in J/K) is the Boltzmann constant, T is the absolute temperature (Gittes and Schmidt, 1998). The thermal force can modeled as (Kim and Zydney, 2004)

$$F_t = \delta(2\sigma k_B T/T_s)^{1/2} \tag{3}$$

where δ is the white noise with zero mean and unit variance, and T_s is the sampling time. Single-sided PSDs are considered, that is, the particle will undergo free diffusion in water when only excited by the thermal force ($F_x = 0$).

The gravitational force due to the gravity and buoyancy can be given by (Hejazian et al., 2015)

$$F_g = -V_p(\rho_p - \rho_f)g \tag{4}$$

where V_p, ρ_p, ρ_f, and g are the particle volume, the particle density, fluid density, and the acceleration of gravity, respectively.

Some other forces can also have an effect on the microparticle including lift force, particle–particle interaction force, magnetic interaction force, van der Waals attraction force, thermophoretic force, and electrostatic interaction force between particles. Depending on the application, some of these forces can be added to the model.

While there exist various forces acting on the micro-particle, it is possible to neglect most of these forces depending on the particle size, working environment, and magnetic force level. Since the electromagnets produce a relatively high magnetic field, the magnetic force and the drag force are the most dominant forces for magnetic particles whose diameter is around 1 to 10 μm (Hejazian et al., 2015), and thus, all other forces might be neglected in system design and analysis. Specifically, the magnetic force must be generated adequately to satisfy desired control actions because it is the control input of the magnetic particle dynamics given in (1).

Magnetic force on a magnetic particle

The magnetic force acting on a magnetic particle is dependent on the magnetic moment m(in Am^2) and the gradient of magnetic flux density B(in T). The magnetic moment (or the magnetic force acting on a point-like magnetic dipole) can be written as the derivative of the magnetic energy (Nguyen, 2012)

$$\vec{F} = \nabla(\vec{m} \cdot \vec{B})/2 = (\vec{m} \cdot \nabla)\vec{B}/2 \tag{5}$$

The second part of the equation holds when the magnetic moment of the particle is not varying in space (i.e. no current density on the particle). This expression is a strong function of spatial coordinates. The magnetic dipole moment of a weakly magnetic particle can be given by (Shevkoplyas et al., 2007)

$$\vec{m} = V_b\vec{M} \tag{6}$$

where $\vec{M} = \chi\vec{H}$ is the magnetization of the particle, χ is the susceptibility, and V_b is the volume of the particle. Since in a diamagnetic medium (e.g. water) the magnetic flux density is defined as $\vec{B} = \mu_0\vec{H}$, where $\vec{H}$ is the magnetic field intensity, by substituting (6) into (5) the force can be written as

$$\vec{F} = \frac{V_b\chi}{2\mu_0}(\vec{B} \cdot \nabla)\vec{B} \tag{7}$$

To calculate the magnetic force, the components of the magnetic field vector are needed to be known. On the other hand, the magnetic force calculations can be specified and simplified by using some assumptions, that is, using the empirical results and magnetic dipole (point magnetic charge) approach. The magnetization or magnetic moment of the magnetic particles have been determined experimentally in some studies (Fonnum et al., 2005).

While equation (7) can be used for force calculations, the effect of demagnetization field should be included in the magnetization process. When a particle is magnetized by an external magnetic field, a self-field develops within the particle that opposes to the external magnetic field. This effect is called the demagnetizing field and defined by (Furlani, 2001)

$$\vec{H}_{in} = \vec{H} + \vec{H}_d \tag{8}$$

where the demagnetizing field is given by $\vec{H}_d = -N\vec{M}$ for the sphere's demagnetizing factor $N = 1/3$. The magnetization of the sphere is defined by $\vec{M} = \chi\vec{H}_{in}$ with $\chi = (\mu - \mu_0)/\mu_0$. Hence,

$$\vec{H}_{in} = \frac{3\mu_0}{\mu + 2\mu_0}\vec{H} \tag{9}$$

The magnetization inside the particle is then

$$\vec{M} = \chi\vec{H}_{in} = \frac{3(\mu - \mu_0)}{(\mu + 2\mu_0)}\vec{H} \tag{10}$$

The magnetic moment of a magnetic particle is then obtained as

$$\vec{m} = V_b\vec{M} = \frac{3V_b}{\mu_0}\frac{(\mu - \mu_0)}{(\mu + 2\mu_0)}\vec{B} \tag{11}$$

where μ is the permeability of the magnetic particle and V_b is the volume of the particle.

Now, the magnetic field $\vec{B}$ must be specified to calculate the magnetic force. By considering the tip of the pole as a point magnetic charge (or pole), as shown in Figure 4, the generated magnetic field at a position $\vec{r}$ by the magnetic charge q can be given by

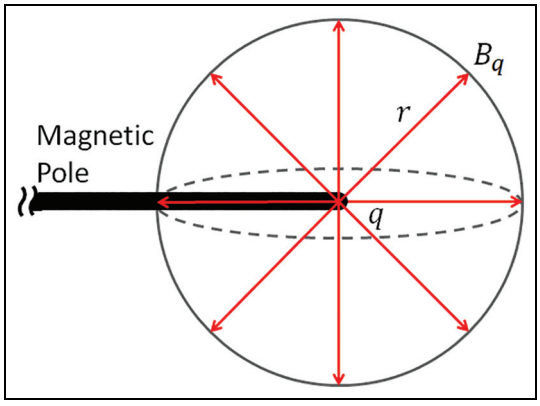

Figure 4. Magnetic monopole approach.

$$\vec{B} = \frac{\mu_0 q}{4\pi r^2}\frac{\vec{r}}{r} \tag{12}$$

where $\vec{r}$(in m) is the vector originated from the location of the magnetic charge to the magnetic particle, q(in A · m) is the magnetic charge, and the total magnetic field is the superposition of the magnetic fields of independent electromagnets. For a single magnetic charge, the magnetic field can be given by

$$\vec{B} = k_m\frac{q}{r^2}\hat{u} \tag{13}$$

where $\hat{u}$ is the unit directional vector (in x or y direction), and $k_m = \mu_0/4\pi$. Therefore, the generated force can be written as

$$\vec{F} = \frac{3V_b}{2\mu_0}\frac{\mu - \mu_0}{\mu + 2\mu_0}\nabla(\vec{B}\cdot\vec{B}) = k_Q\nabla(\vec{B}\cdot\vec{B}) \tag{14}$$

where $k_Q = 3V_b(\mu - \mu_0)/(2\mu_0(\mu + 2\mu_0))$. Substituting (13) into (14) and arranging into a quadratic form

$$\vec{F}_u = k_Q\nabla\left(k_m^2\frac{q^2}{r^4}[\hat{u}\cdot\hat{u}]\right) = \frac{4k_Qk_m^2}{d^5}q^2\hat{u} \tag{15}$$

where $r = d$(in m) is the distance between pole tip and workspace center. Now we need to define the magnetic charge q. The relation between magnetic charge q and magnetic flux ϕ is given by

$$q = \phi/\mu_0 \tag{16}$$

By considering the magnetic circuit, the electromagnets based magnetic actuator is characterized by reluctance R_a, magnetomotive force N_cI_i, magnetic flux ϕ_i, and pole face area A_a for $i = 1, 2$. The lumped reluctance of air gap between the pole tip and the working area center is defined with R_a. Because the pole is made of strong magnetic materials than air, it is possible to ignore the effects of these materials to simplify the calculations. Since all electromagnets are identical, the implementation of the Ampere's loop law to magnetic circuit results in

$$\phi_i = N_cI_i/R_a \tag{17}$$

where N_c is the number of wire turns of the coils, and the air gap reluctance is

$$R_a = \frac{g_a}{\mu_0A_a} \tag{18}$$

where the permeability of air is given by $\mu_0 = 4\pi \times 10^{-7}$(in T·m/A), g_a(in m) is the air gap length, and A_a(in m^2) is the cross-section area.

By substituting the magnetic flux ϕ given in (17) into the equation (16), we get

$$q = \phi/\mu_0 = N_cI/(\mu_0R_a) \tag{19}$$

Substituting (19) into force equation (15), the magnetic force model for each electromagnet is obtained as

$$\vec{F}_u = \left(\frac{4k_Qk_m^2}{d^5}\right)\left(\frac{N_c}{\mu_0R_a}\right)^2I^2\hat{u} \tag{20}$$

It is clear that, by considering forces of all magnets, the magnetic force at the center of workspace ($x = 0$) can be written as

$$F_x = k_{ii}\left(I_1^2 - I_2^2\right) \tag{21}$$

with

$$k_{ii} = \left(\frac{4k_Q k_m^2}{d^5}\right)\left(\frac{N_c}{\mu_0 R_a}\right)^2 \tag{22}$$

The model is simplified by eliminating the spatial dependence.

Model analysis

The electromagnets are designed with the same parameters and symmetrically located to pull the superparamagnetic particle in x-direction. The working area has a length of d from center to pole tip, and the position of superparamagnetic particle is defined in the range of $x \in [-d, d]$ in x-direction. By considering the model (1), the mass of the magnetic particle is around $m \sim 10^{-15}$ kg, and damping coefficient is around $\sigma \sim 10^{-7}$ Ns/m, hence the inertia force $m\ddot{x}$ is much smaller than the drag force $\sigma\dot{x}$, and the inertia force may be neglected in the analysis. For this reason, the magnetic particle model might further be simplified as

$$\sigma\dot{x} = F_x + F_T \tag{23}$$

where F_T (in N) is the sum of other forces. Hence the system is a type-1 system or an integrating system. Namely, the open-loop system does not naturally settle out at a steady-state operating point. Integrating systems can be remarkably challenging to control, but if the aim of the controller is to find the input required to force the output to match a setpoint, a P-control method can work well.

The other significant part of the system is related to the dynamic behavior of the electromagnets. The electrical model of electromagnets can be written as

$$L\frac{dI_i}{dt} + RI_i = V_i \tag{24}$$

where the parameters of the electrical part of the system model are assumed to be equal due to the symmetric and identical coil designs, in which L (in Henry) is the coil inductance, R (in Ohm) is the coil resistance and V_i (in V) is the applied control voltage. It should be noted that the electromagnets are composed of fast, stable, and linear electrical dynamics, with a time constant $\tau_e = L/R \approx 5x10^{-3}$ s, so the effects of the electrical dynamics are ignored in the design and analysis.

A feedback linearizing controller design using offset current

A state feedback controller can be defined by using an offset current to effectively linearize the magnetic force model. Offset current based control design is based on changing

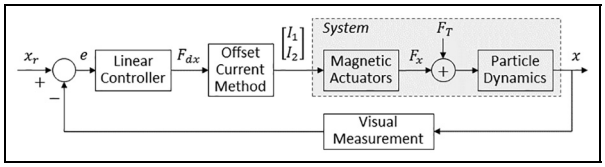

Figure 5. A feedback linearizing controller using offset current.

variables with respect to the electromagnet currents. First, consider the magnetic force to current relation equation (21). Then, define current variables i_0 and i_c such that

$$\begin{aligned} I_1 &= (i_0 + i_c)/2 \\ I_2 &= (i_0 - i_c)/2 \end{aligned} \tag{25}$$

Substituting (25) into (21), the force becomes

$$F_x = k_{ii} i_0 i_c \tag{26}$$

Now, when the magnitude of i_0 is kept constant (e.g., $i_0 = 1$ A) and i_c is varying with magnetic force, any force can be realized. The electromagnet currents are then

$$\begin{aligned} I_1 &= (i_0 + F_{dx}/(k_{ii} i_0))/2 \\ I_2 &= (i_0 - F_{dx}/(k_{ii} i_0))/2 \end{aligned} \tag{27}$$

where F_{dx} is the desired magnetic force. It is clear that the offset current control method provides simple linear control signals whose magnitudes vary with desired force values. The value of offset current must be selected carefully to avoid amplifier saturation and possibly instability. The block diagram of the controlled system is illustrated in Figure 5. Since the open-loop system is a type-1 system, a desired setpoint following magnetic force value can be obtained with a P-controller by

$$F_{dx} = k_p(x_r - x) \tag{28}$$

where k_p is the proportional control gain, x_r is a constant position reference, and x is the measured position.

Since the controller linearizes the system, the linear analysis methods can be used for stability analysis of the closed-loop system. By substituting (27) into (23), the closed loop system becomes

$$m\ddot{x} + \sigma\dot{x} = F_{dx} + F_T \tag{29}$$

By taking Laplace transform of (29) with the controller (28), we get the closed-loop transfer function as

$$X(s) = \frac{1}{ms^2 + \sigma s + k_p}\left[k_p X_r(s) + F_T(s)\right] \tag{30}$$

From (30), the closed-loop system is stable if $k_p > 0$. By considering the simplified model (23), the control gain can be calculated for a desired time constant τ_d (in s) as $k_p = \sigma/\tau_d$.

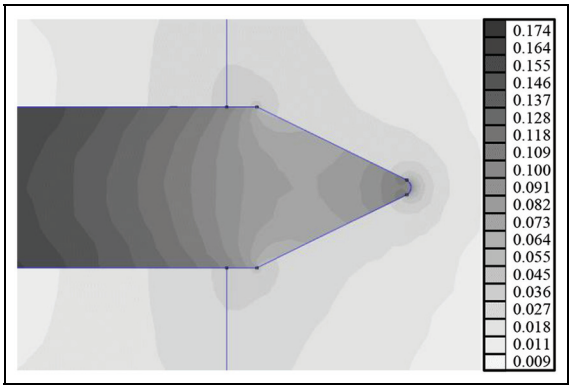

Figure 6. Magnetic flux density of an electromagnet, B (Tesla).

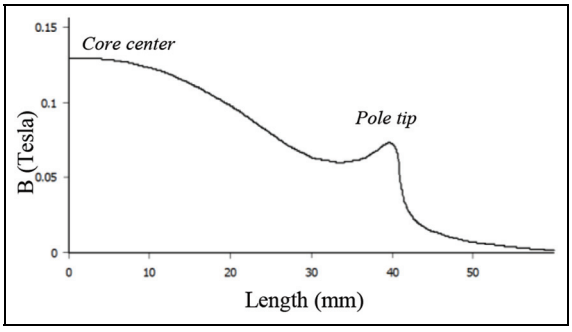

Figure 7. Distribution of the magnetic flux density.

Results

To get the suitable design for micromanipulation of a superparamagnetic particle, the COMSOL Multiphysics software is used as an advanced finite element numerical solver. In the final design, the coil is designed to have 2000 copper turns with a core of 75 mm length. The core is built with a Nickel-Iron alloy material due to its strong magnetic permeability and high saturation values (Davis, 2001). Different types of materials, such as Mu-metal, are considered as core material, but the Nickel-Iron alloy is used due to its low-cost price, easy accessibility, and high magnetic saturation current. The superparamagnetic particle has a radius of 5 μm, and the distance between the particle and coil tip is around 5 mm. The tip of the core material is designed to be circular. The magnetic flux density of an electromagnet is shown in Figures 6 and 7. It is seen that the magnetic flux density is strong at the core tip, but it decreases as a function of $\sim d^3$ in the diamagnetic environment as seen in Figure 7.

A photo of the experimental setup of the horizontal magnetic micromanipulator is given in Figure 8. The superparamagnetic particles are controlled in a workspace whose radius is 500 μm. The sampling rate of the industrial camera is 53 frames per second (when the camera resolution is 640x480 pixels). The magnetic microparticle is detected as a circle with a particle detection and tracking algorithm, which is seen on the computer screen in Figure 8. An adjustable multichannel

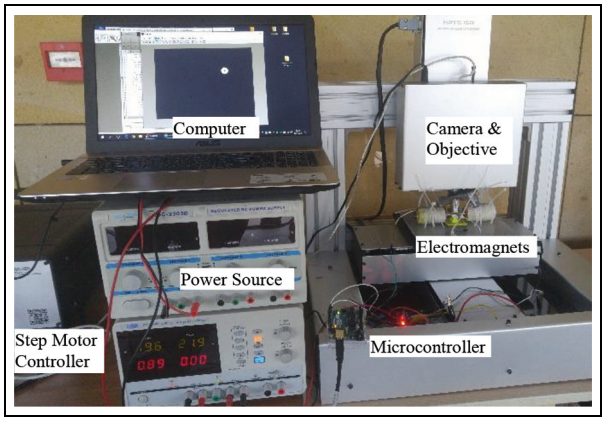

Figure 8. The experimental setup.

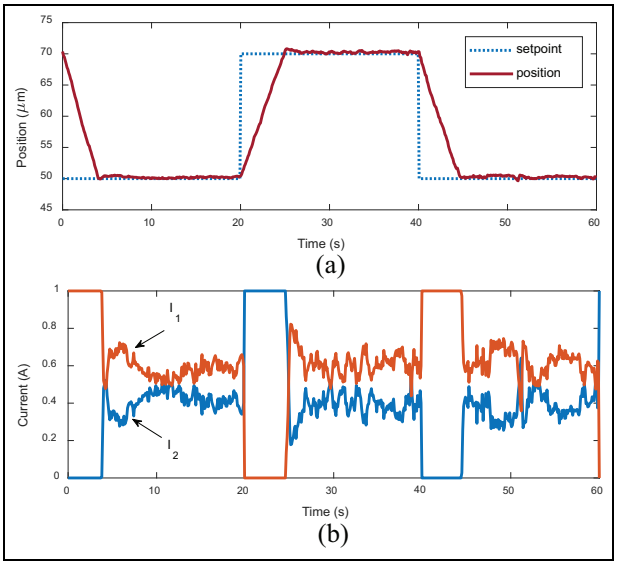

Figure 9. Experimental control results for step setpoint, (a) particle position and (b) control currents.

DC power supply with 0-30 V and 0-3 A outputs, power MOSFET driver circuits and PWM outputs of a microcontroller are used to produce the time-varying currents to control the electromagnets. The other details of the system are explained in Section 3.1.

The horizontal position control experiments are done with step and sinusoidal setpoints. Figure 9 shows the step response of the horizontal micromanipulator. The model parameters are calculated as $k_{ii} = 2.42 \times 10^{-13}$ N/A^2 and $\sigma = 2 \times 10^{-7}$ Ns/m. Hence, for a time constant of $\tau_d = 0.25$ seconds, the control gain is found to be $k_p = 0.8 \times 10^{-6}$ N/m. The applied current is limited to $1\,A$ to protect the system from magnetic material saturation and hysteresis heating. This limitation yields a 24 pN maximum magnetic force on a superparamagnetic particle and a 5 $\mu m/s$ particle velocity as seen in Figure 9a. This magnetic force and speed of magnetic particle can be increased with design parameters including

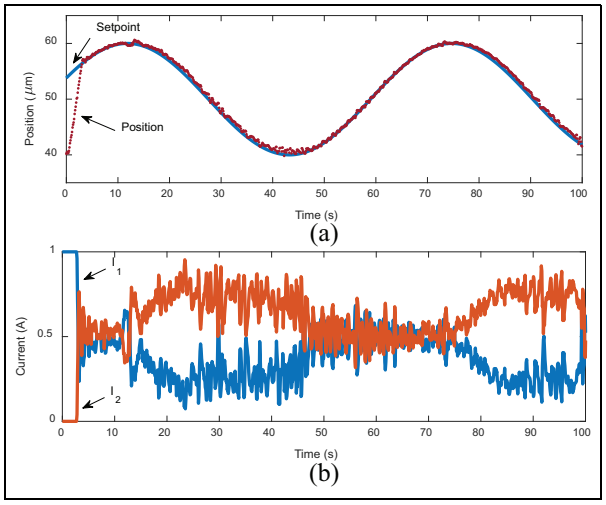

Figure 10. Experimental control results for sinusoidal setpoint, (a) particle position and (b) control currents.

core material (stronger magnetic materials), distance between core tip and the particle (smaller distance), and number of copper turns (larger number of turns). When the particle is in the close neighborhood of the setpoint, the time constant requirement is satisfied. That is, the proposed controller has a non-overshoot response with 1 second settling time and smooth control signals. The applied current signals stay around 0.5 A when the particle reaches its steady-state conditions. The measurement plus thermal noise level is around $\pm 0.25\ \mu m$, which causes fluctuations on the current signals. The random thermal noise force exists due to the impacts of the molecules of the liquid on the particle and its effect increases with temperature. At room temperature conditions, the thermal noise force will always be a factor and it cannot be eliminated, but an observer (Ablay and Aldemir, 2013) may be designed to estimate this force to use in feedback to decrease its effect. In our experiments, the electromagnet temperature reached to 35–40°C, so a cooling mechanism may be considered to decrease the thermal noise level. The similar results are obtained for the sinusoidal setpoint as seen in Figure 10. While the controller is designed for tracking constant setpoints, it is seen from Figure 10 that the possible time-varying setpoint tracking requirements can also be met with the proposed controller. It is clear from experimental results that the proposed controller provides a highly satisfactory control performance with zero steady-state error.

Conclusion

A full automatic horizontal magnetic micromanipulator is developed and implemented in aqueous solution to manipulate superparamagnetic particles. A dynamic model of the system is developed using magnetic monopole and magnetic circuit approaches, and this model is used to develop a feedback linearizing controller for precise positioning. A visual particle detecting and tracking algorithm is developed to measure the position of the target superparamagnetic particle. The proposed controller benefits from system model, offset current, and linear controller, and effectively eliminates the input nonlinearity and position dependency of the micromanipulator to perform a satisfying control performance within the workspace. The applied control current is limited to maximum 1 A to avoid saturation and hysteresis of magnetic materials. The magnetic micromanipulator is able to generate up to 24 pN force on the magnetic particle whose radius is less than 5 μm, which allows a full automatic control in the workspace with a maximum particle speed of 5 μm/s at the center. The developed system can be used in applications in cell/molecule manipulation, DNA extraction and biosensors.

Declaration of conflicting interests

The author(s) declared no potential conflict of interests with respect to the research, authorship and/or publication of this article.

Funding

The author(s) disclosed receipt of the following financial support for the research, authorship, and/or publication of this article: This work was supported by Turkish Scientific and Research Council (TUBITAK) under project number 116E168.

ORCID iD

Günyaz Ablay https://orcid.org/0000-0003-2862-6761

References

Ablay G and Aldemir T (2013) Fault detection in nuclear systems using sliding mode observers. *Nuclear Science and Engineering* 173(1): 82–98.

Agostini A, Kircher M, Do R, et al. (2016) MR imaging of the liver (including biliary contrast agents). *Semin Roentgenol* 51: 308–316.

Aziz MS, Jalil MA, Suwanpayak N, et al. (2012) Optical manipulation of nano-micro needle array for large volume molecular diagnosis. *Artificial Cells, Blood Substitutes, and Immobilization Biotechnology* 40(4): 266–270.

Capitanio M and Pavone FS (2013) Interrogating biology with force: Single molecule high-resolution measurements with optical tweezers. *Biophysical Journal*. 105(6): 1293–1303.

Davis JR (2001) *ASM Specialty Handbook: Nickel, Cobalt, and Their Alloys*. Ohio: ASM International.

Eroglu Y and Ablay G (2016) Cascade sliding mode–based robust tracking control of a magnetic levitation system. Proceedings of the Institution of Mechanical Engineers, Part I. *Journal of Systems and Control Engineering* 230(8): 851–860.

Fabian R, Tyson C, Tuma PL, et al. (2018) A horizontal magnetic tweezers and its use for studying single DNA molecules. *Micromachines* 9(4): 188–200.

Fonnum G, Johansson C, Molteberg A, et al. (2005) Characterisation of Dynabeads® by magnetization measurements and Mössbauer spectroscopy. *Proceedings of the Fifth International Conference on Scientific and Clinical Applications of Magnetic Carriers. Journal of Magnetism and Magnetic Materials* 293(1): 41–47.

Fuller DN, Gemmen GJ, Rickgauer JP, et al. (2006) A general method for manipulating DNA sequences from any organism with optical tweezers. *Nucleic Acids Res* 34(2): e15.

Furlani EP (2001) *Permanent Magnet and Electromechanical Devices: Materials, Analysis, and Applications*, 1 edition. San Diego: Academic Press.

Gijs MAM (2004) Magnetic bead handling on-chip: New opportunities for analytical applications. *microfluidics and nanofluidics* 1(1): 22–40.

Gittes F and Schmidt CF (1998) Thermal noise limitations on micromechanical experiments. *Eur Biophys J* 27(1): 75–81.

Gosse C and Croquette V (2002) Magnetic tweezers: Micromanipulation and force measurement at the molecular level. *Biophysical Journal* 82(6): 3314–3329.

Happel J and Brenner H (1983) L*ow Reynolds Number Hydrodynamics: With Special Applications to Particulate Media. Mechanics of Fluids and Transport Processes*. Netherlands: Springer.

Hejazian M, Li W and Nguyen N-T (2015) Lab on a chip for continuous-flow magnetic cell separation. *Lab Chip* 15(4): 959–970.

Hermanson GT (2013) *Bioconjugate Techniques* (3rd edn). Waltham, MA: Academic Press, London.

Huhle A, Klaue D, Brutzer H, et al. (2015) Camera-based three-dimensional real-time particle tracking at kHz rates and Ångström accuracy. *Nature Communications* 6(5885): 1–8.

İçöz K and Mzava O (2016) Detection of proteins using nano magnetic particle accumulation-based signal amplification. *Applied Sciences* 6(12).

Icoz K and Savran C (2010) Nanomechanical biosensing with immunomagnetic separation. *Applied Physics Letters* 97(12): 123701(1–3).

Jokerst JV, Chen Z, Xu L, et al. (2015) A magnetic bead-based sensor for the quantification of multiple prostate cancer biomarkers. *PLoS ONE* 10(9): 1–15.

Ju L and Zhu C (2017) Benchmarks of biomembrane force probe spring constant models. *Biophysical Journal* 113(12): 2842–2845.

Kim DK, Mikhaylova M, Wang FH, et al. (2003) Starch-coated superparamagnetic nanoparticles as mr contrast agents. *Chemistry of Materials* 15(24): 4343–4351.

Kim M and Zydney AL (2004) Effect of electrostatic, hydrodynamic, and Brownian forces on particle trajectories and sieving in normal flow filtration. *Journal of Colloid and Interface Science* 269(2): 425–431.

Klaue D and Seidel R (2009) Torsional stiffness of single superparamagnetic microspheres in an external magnetic field. *Phys. Rev. Lett.* 102(20): 028302.

Kodama T, Osaki T, Kawano R, et al. (2013) Round-tip dielectrophoresis-based tweezers for single micro-object manipulation. *Biosensors and Bioelectronics* 47: 206–212.

Kriegel F, Ermann N and Lipfert J (2017) Probing the mechanical properties, conformational changes, and interactions of nucleic acids with magnetic tweezers. *Journal of Structural Biology, Molecular Forces to Cellular Function* 197(1): 26–36.

Lawaczeck R, Bauer H, Frenzel T, et al. (1997) Magnetic iron oxide particles coated with carboxydextran for parenteral administration and liver contrasting. Pre-clinical profile of SH U555A. *Acta Radiologica* 38(4): 584–597.

Li M, Xiao X, Liu L, et al. (2013) Atomic force microscopy study of the antigen-antibody binding force on patient cancer cells based on ROR1 fluorescence recognition. *Journal of molecular recognition* 26(9): 432–438.

Litvinov RI, Shuman H, Bennett JS and Weisel JW (2002) Binding strength and activation state of single fibrinogen-integrin pairs on living cells. *Proceedings of the National Academy of Sciences of the United States of America* 99(11): 7426–7431.

Luo H, Sun W and Yeow JT (2018) Modelling and adaptive dynamic sliding mode control of dielectrophoresis-based micromanipulation. *Transactions of the Institute of Measurement and Control* 40(1): 122–134.

McAndrew CP, Tyson C, Zischkau J, et al. (2016) Simple horizontal magnetic tweezers for micromanipulation of single DNA molecules and DNA—protein complexes. *BioTechniques* 60(1): 21–27.

Neuman KC and Nagy A (2008) Single-molecule force spectroscopy: optical tweezers, magnetic tweezers and atomic force microscopy. *Nature Methods* 5(1): 491–505.

Nguyen N-T (2012) Micro-magnetofluidics: interactions between magnetism and fluid flow on the microscale. *Microfluid Nanofluid* 12(1): 1–16.

Nguyen VQ, Ahmed AS and Ramanujan RV (2012) Morphing soft magnetic composites. *Adv. Mater. Weinheim* 24(30): 4041–4054.

Pelz B, Žoldák G, Zeller F, et al. (2016) Subnanometre enzyme mechanics probed by single-molecule force spectroscopy. *Nature Communications* 7(10848): 1–9.

Plouffe BD, Murthy SK and Lewis LH (2015) Fundamentals and application of magnetic particles in cell isolation and enrichment: A review. *Reports on Progress in Physics* 78(1): 016601(1–30).

Prass M, Jacobson K, Mogilner A and Radmacher M (2006) Direct measurement of the lamellipodial protrusive force in a migrating cell. *The Journal of Cell Biology* 174(6): 767–772.

Rahman M, Saei A, Amiri H and Mahmoudi M (2015) Biomedical applications of superparamagnetic nanoparticles in molecular scale. *Current Organic Chemistry* 19(11): 982–990.

Rosensweig RE (2002) Heating magnetic fluid with alternating magnetic field. Proceedings of the 9th International Conference on Magnetic Fluids. *Journal of Magnetism and Magnetic Materials* 252: 370–374.

Schwarz FW, Tóth J, van Aelst K, et al. (2013) The helicase-like domains of Type III restriction enzymes trigger long-range diffusion along DNA. *Science* 340(6130): 353–356.

Shevkoplyas SS, Siegel AC, Westervelt RM, et al. (2007) The force acting on a superparamagnetic bead due to an applied magnetic field. *Lab Chip* 7(10): 1294–1302.

Smith SB, Finzi L and Bustamante C (1992) Direct mechanical measurements of the elasticity of single DNA molecules by using magnetic beads. *Science* 258(5085): 1122–1126.

Stauffer PR, Cetas TC, Fletcher AM, et al. (1984) Observations on the use of ferromagnetic implants for inducing hyperthermia. *IEEE Transactions on Biomedical Engineering BME* 31(1): 76–90.

Strick T, Allemand J-F, Croquette V and Bensimon D (2000) Twisting and stretching single DNA molecules. *Progress in Biophysics and Molecular Biology, Single Molecule Biochemistry and Molecular Biology* 74(1): 115–140.

Svoboda K and Block SM (1994) Force and velocity measured for single kinesin molecules. *Cell* 77(5): 773–784.

Tietze R, Zaloga J, Unterweger H, et al. (2015) Magnetic nanoparticle-based drug delivery for cancer therapy. *Biochemical and Biophysical Research Communications, Nanomedicine* 468(3): 463–470.

Vlaminck ID and Dekker C (2012) Recent advances in magnetic tweezers. *Annual Review of Biophysics* 41(1): 453–472.

Yan J, Skoko D and Marko JF (2004) Near-field-magnetic-tweezer manipulation of single DNA molecules. *Physical Review E, Statistical, Nonlinear, and Soft Matter Physics* 70(1): 011905(1–5).